Bioorganic & Medicinal Chemistry Letters 23 (2013) 6474–6480

Contents lists available at ScienceDirect

Bioorganic & Medicinal Chemistry Letters

journal homepage: www.elsevier.com/locate/bmcl

Synthesis, structure analysis, antitumor evaluation and 3D-QSAR studies of 3,6-disubstituted-dihydro-1,2,4,5-tetrazine derivatives

Guo-Wu Rao [a,*], Cui Wang [a], Jian Wang [b], Zhen-Guo Zhao [a], Wei-Xiao Hu [a]

[a] College of Pharmaceutical Science, Zhejiang University of Technology, Hangzhou 310014, People's Republic of China
[b] School of Pharmaceutical Engineering, Shenyang Pharmaceutical University, Shenyang 110016, People's Republic of China

ARTICLE INFO

Article history:
Received 26 March 2013
Revised 25 August 2013
Accepted 11 September 2013
Available online 20 September 2013

Keywords:
Tetrazine
X-ray diffraction
Antitumor activity
3D-QSAR
CoMFA
CoMSIA

ABSTRACT

3,6-Diaryl-dihydro-1,2,4,5-tetrazine derivatives were synthesized and their structures were confirmed by single-crystal X-ray diffraction. Monosubstituted dihydrotetrazines are the 1,4-dihydro structure, but disubstituted dihydrotetrazines are the 1,2-dihydro structure. The results of further research indicated there may be a rearrangement during the synthesis process of disubstituted dihydrotetrazines. Their antitumor activities were evaluated against A-549 and P388 cells in vitro. The results showed several compounds to be endowed with cytotoxicity in the low micromolar range. Two compounds were highly effective against A-549 cell and IC_{50} values were 0.575 and 2.08 μM, respectively. Three-dimensional quantitative structure–activity relationship (3D-QSAR) studies of comparative molecular field analysis (CoMFA) and comparative molecular similarity indices analysis (CoMSIA) were carried out on 37 1,2,4,5-tetrazine derivatives with antitumor activity against A-549 cell. Models with good predictive abilities were generated with the cross validated q^2 values for CoMFA and CoMSIA being 0.744 and 0.757, respectively. Conventional r^2 values were 0.978 and 0.988, respectively, the predicted R^2 values were 0.916 and 0.898, respectively. The results provide the tool for guiding the design and synthesis of novel and more potent tetrazine derivatives.

1,2,4,5-Tetrazine derivatives have a high potential for biological activity, such as anti-mite activity,[1] herbicidal activity,[2] antimalarial activity,[3] antiviral activity,[4] antiinflammatory activity,[5] antibacterial activity,[6] and antitumor activity.[7–10] 1,2,4,5-Tetramethyl-3,6-bis(phenylethynyl)-1,2,4,5-tetrazine[10] had been described as an antitumor compound. It was the original expression that 1,2,4,5-tetrazine derivatives may possess antitumor activity. The report had attracted interests from researchers, and the cytotoxicity has also been studied in recent years.[11–13]

Quantitative structure–activity relationship (QSAR) modeling results in a quantitative correlation between chemical structure and properties (such as biological activity), it can be also applied to predict biological activity of nonsynthesized compounds structurally related to a training set of compounds. Among techniques of three-dimensional quantitative structure–activity relationship (3D-QSAR), comparative molecular field analysis (CoMFA) and comparative molecular similarity indices analysis (CoMSIA) are two powerful prevailing methodologies,[14,15] which are the most widely used for the study of compounds with potential biological activity.

In our continuous effort to develop potential antitumor agents,[12,16–20] we researched the synthesis, structure analysis, biological evaluation of 1,2,4,5-tetrazine compounds and attempted to investigate whether modifications to this structure could enhance antitumor activities of this compound class. In this Letter, nineteen 3,6-diaryl-dihydro-1,2,4,5-tetrazine derivatives (**1** and **2**) were synthesized from 3,6-diaryl-1,4-dihydro-1,2,4,5-tetrazine (**3**) and alkyl chloroformate under pyridine as a catalyst. The synthetic route is shown in Scheme 1.[21] The intermediate raw material of compound **3** was prepared to accord to the published method.[16] The results are summarized in Table 1. There seems to be considerable confusion over the structures of 1,2- and 1,4-dihydro-1,2,4,5-tetrazine isomers, and the same compound is often formulated as both structures. In most cases, the dihydro structure, which would be the initial reaction product, is presented, or the authors have formulated their compounds in the dihydro structure, which appeared to be the most accepted at that time.[12] So their structures were further confirmed by single-crystal X-ray diffraction.

Single-crystal structures of compound **1g** and **2g** were determined by X-ray crystallography,[22,23] and their molecular structures are illustrated in Figures 1 and 2, respectively. In the molecule of **1g** (Fig. 1), the N2═C3 [1.286(2) Å] and N5═C6 [1.273(2) Å] bonds correspond to typical C═N double-bond lengths, and the C3–N4 [1.372(2) Å], N4–N5 [1.396(2) Å], C6–N1 [1.420(2) Å], and N1–N2 [1.428(2) Å] bond lengths correspond to typical single bonds. Therefore, the tetrazine ring is the 1,4-dihydro structure with the

* Corresponding author.
E-mail address: rgw@zjut.edu.cn (G.-W. Rao).

0960-894X/$ - see front matter © 2013 Elsevier Ltd. All rights reserved.
http://dx.doi.org/10.1016/j.bmcl.2013.09.036

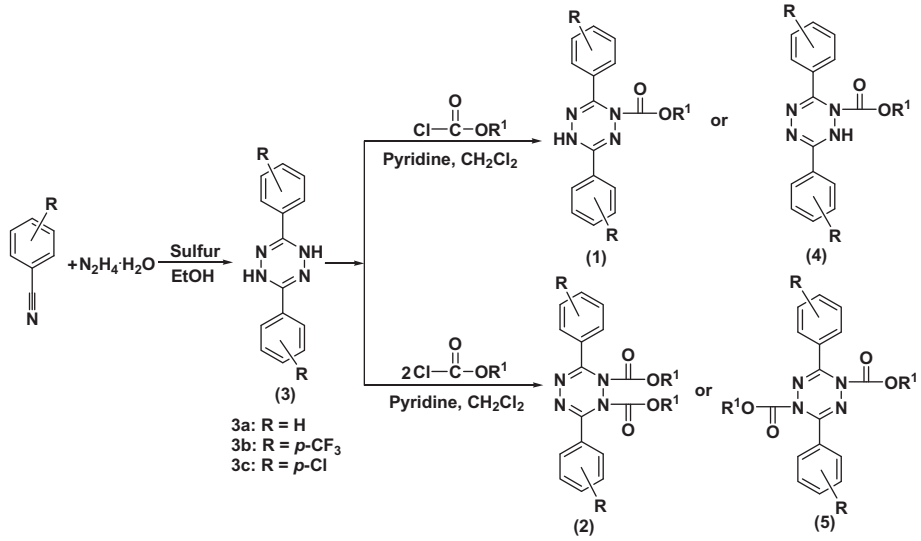

Scheme 1. Route of synthesis.

N-substituted group at the 1-position and the N-hydrogen at the 4-position; the compound is methyl 3,6-bis(4-trifluoromethylphenyl)-1,4-dihydro-1,2,4,5-tetrazine-1-carboxylate (**1g**), rather than methyl 3,6-bis(4-trifluoromethylphenyl)-1,2-dihydro-1,2,4,5-tetrazine-1-carboxylate (**4g**). In the molecule of **2g** (Fig. 2), the C3═N4 [1.276(4) Å] and N5═C6 [1.288(4) Å] bonds correspond to typical C═N double-bond lengths, and the N2–C3 [1.437(4) Å], N4–N5 [1.400(4) Å], C6–N1 [1.411(3) Å], and N1–N2 [1.393(3) Å] bond lengths correspond to typical single bonds. Therefore, the tetrazine ring is 1,2-dihydro structure with the

Table 1
Synthesis of compound **1** and **2**

Compd	R	R^1	Yield (%)	Time (h)	Mp (°C)	^{1}H NMR (400 MHz, $CDCl_3$, ppm)
1a	H	Me	70.2	3	164(d)	3.79 (s, 3H), 7.38–7.47 (m, 5H), 7.52–7.58 (m, 3H), 7.77 (d, *J* = 7.6 Hz, 2H), 7.96 (s, 1H)
1b	H	Et	61.3	24	138–140	1.12 (t, *J* = 6.9 Hz, 3H), 4.20 (q, *J* = 7.0 Hz, 2H), 7.37–7.42 (m, 5H), 7.48–7.57 (m, 3H), 7.76 (d, *J* = 7.9 Hz, 2H), 8.15 (s, 1H)
1c	H	*n*-Pr	82.5	20	141–142	0.72 (t, *J* = 7.4 Hz, 3H), 1.45–1.50 (m, 2H), 4.09 (t, *J* = 6.6 Hz, 2H), 7.36–7.41 (m, 5H), 7.50–7.58 (m, 3H), 7.74–7.77 (m, 2H), 8.17 (s, 1H)
1d	H	*n*-C_5H_{11}	11.2	40	92–94	0.82 (t, *J* = 7.3 Hz, 3H), 1.05-1.08 (m, 2H), 1.17-1.23 (m, 2H), 1.42-1.46 (m, 2H), 4.12 (t, *J* = 6.6 Hz, 2H), 7.38–7.46 (m, 5H), 7.51–7.58 (m, 3H), 7.77–7.79 (m, 2H), 7.96 (s, 1H)
1e	H	*i*-C_5H_{11}	7.9	24	129–130	0.79 (d, *J* = 6.0 Hz, 6H), 1.33 (m, 2H), 1.63 (m, 1H), 4.16 (t, *J* = 6.3 Hz, 2H), 7.38–7.48 (m, 5H), 7.51–7.57 (m, 3H), 7.78 (d, *J* = 7.3 Hz, 2H), 7.93 (s, 1H)
1f	H	$ClCH_2CH_2$	21.6	40	164–165	3.51 (t, *J* = 5.8 Hz, 2H), 4.37 (t, *J* = 6.0 Hz, 2H), 7.39–7.46 (m, 5H), 7.52–7.59 (m, 3H), 7.76–7.78 (m, 2H), 8.07 (s, 1H)
1g	*p*-CF_3	Me	53.7	24	198–199	3.83 (s, 3H), 7.67–7.73 (m, 6H), 7.89–7.91 (m, 2H), 8.07 (s, 1H)
1h	*p*-CF_3	Et	44.1	54	194–195	1.15 (t, *J* = 7.0 Hz, 3H), 4.23 (q, *J* = 7.1 Hz, 2H), 7.66–7.72 (m, 6H), 7.90–7.92 (m, 2H), 8.12 (s, 1H)
1i	*p*-CF_3	*n*-Pr	24.4	23	181–182	0.74 (t, *J* = 7.2 Hz, 3H), 1.51-1.58 (m, 2H), 4.12 (t, *J* = 6.6 Hz, 2H), 7.67–7.76 (m, 5H), 7.82–7.84 (m, 1H), 7.90–7.94 (m, 2H), 8.30 (d, *J* = 8.1 Hz, 1H)
1j	*p*-Cl	Me	65.3	24	211–213	3.80 (s, 3H), 7.37 (d, *J* = 8.5 Hz, 2H), 7.43–7.50 (m, 4H), 7.71 (d, *J* = 8.5 Hz, 2H), 7.89 (s, 1H)
2a	H	Me	67.1	5	182–183[20]	3.74 (s, 6H), 7.48–7.55 (m, 6H), 8.06 (d, *J* = 7.1 Hz, 4H)
2b	H	Et	34.2	9	121–122[20]	1.11 (t, *J* = 7.1 Hz, 6H), 4.12-4.16 (m, 2H), 4.21-4.27 (m, 2H), 7.49–7.58 (m, 6H), 8.08 (d, *J* = 7.0 Hz, 4H)
2c	H	*n*-Pr	63.6	5	111–112[20]	0.64 (t, *J* = 7.2 Hz, 6H), 1.42–1.48 (m, 4H), 3.98-4.04 (m, 2H), 4.11-4.17(m, 2H), 7.47–7.55 (m, 6H), 8.06 (d, *J* = 6.8 Hz, 4H)
2d	H	CH_2–C$_6$H$_{11}$	43.8	15	180–181	0.63-0.65 (m, 4H), 0.96-1.06 (m, 6H), 1.31 (m, 6H), 1.54-1.57 (m, 6H), 3.81-3.82 (m, 2H), 4.00-4.04 (m, 2H), 7.47–7.53 (m, 6H), 8.06 (d, *J* = 6.7 Hz, 4H)
2e	*p*-CF_3	Me	30.5	22	200–202	3.77 (s, 6H), 7.77 (d, *J* = 8.2 Hz, 4H), 8.17 (d, *J* = 8.1 Hz, 4H)
2f	*p*-CF_3	Et	39.6	20	167–169	1.12 (t, *J* = 6.3 Hz, 6H), 4.14-4.27 (m, 4H), 7.77 (d, *J* = 8.2 Hz, 4H), 8.17 (d, *J* = 8.0 Hz, 4H)
2g	*p*-CF_3	*n*-Pr	52.7	16	147–149	0.64 (t, 6H), 1.46-1.48 (m, 4H), 4.04-4.19 (m, 4H), 7.77 (d, *J* = 8.2 Hz, 4H), 8.18 (d, *J* = 8.1 Hz, 4H)
2h	*p*-CF_3	Ph	42.6	42	205–206	7.00 (d, *J* = 7.9 Hz, 4H), 7.23–7.26 (m, 2H), 7.32–7.36 (m, 4H), 7.80 (d, *J* = 8.3 Hz, 4H), 8.30 (d, *J* = 8.1 Hz, 4H)
2i	*p*-CF_3	CH_2–C$_6$H$_{11}$	42.8	18	160–162	0.57–0.63 (m, 4H), 0.91-1.06 (m, 6H), 1.27-1.30 (m, 6H), 1.55-1.58 (m, 6H), 3.81-3.85 (m, 2H), 4.01-4.05 (m, 2H), 7.77 (d, *J* = 8.1 Hz, 4H), 8.18 (d, *J* = 8.0 Hz, 4H)

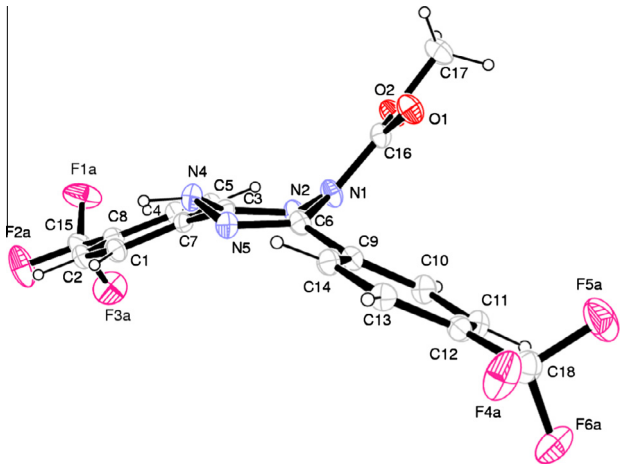

Figure 1. The X-ray crystal structure of compound **1g**, shown with 30% probability displacement ellipsoid.

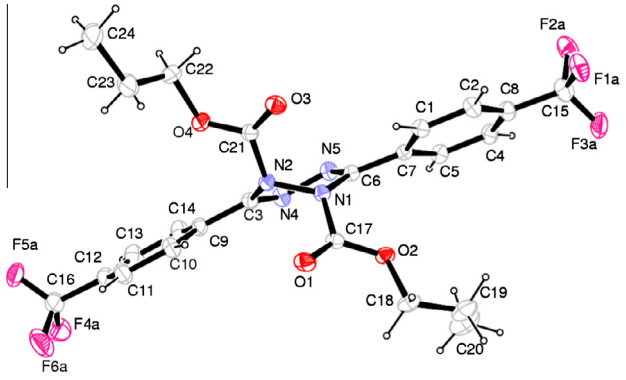

Figure 2. The X-ray crystal structure of compound **2g**, shown with 30% probability displacement ellipsoid.

N-substituted groups at the 1,2-positions and not the 1,4-positions; the compound is dipropyl 3,6-bis(4-trifluoromethylphenyl)-1,2-dihydro-1,2,4,5-tetrazine-1,2-dicarboxylate (**2g**), rather than dipropyl 3,6-bis(4-trifluoromethylphenyl)-1,4-dihydro-1,2,4,5-tetrazine-1,4-dicarboxylate (**5g**).

Therefore, monosubstituted dihydrotetrazines are the 1,4-dihydro structure, but disubstituted dihydrotetrazines are the 1,2-dihydro structure. This is worth to research further. So the reaction of 3,6-diphenyl-1,4-dihydro-1,2,4,5-tetrazine (**3a**) and methyl chloroformate was studied further (Scheme 2). Dimethyl 3,6-diphenyl-1,4-dihydro-1,2,4,5-tetrazine-1,4-dicarboxylate (**6**) as a control was synthesized from the starting material of benzaldehyde. The results indicated the reaction product of methyl 3,6-diphenyl-1,4-dihydro-1,2,4,5-tetrazine-1-carboxylate (**1a**) and methyl chloroformate is dimethyl 3,6-diphenyl-1,2-dihydro-1,2,4,5-tetrazine-1,2-dicarboxylate (**2a**), rather than compound **6**. Therefore, there may be a rearrangement during the synthesis process of compound **2a**.

Table 2
Antitumor activities against A-549 and P388 cell lines in vitro (IC_{50} in μM)

Compd	A-549	P388
1a	39.5	>100
1b	>100	>100
1c	>100	>100
1d	40.8	11.8
1e	44.2	24.6
1f	101	>100
1h	0.575	24.7
1j	49.4	34.9
2a[20]	>100	>100
2b[20]	26.6	11.2
2c[20]	>100	11.7
2d	>100	>100
2e	2.08	30.4
2f	51.1	>100
2g	>100	>100
2h	14.5	26.6
2i	>100	>100

In vitro, antitumor activities of these compounds were evaluated against the growth of A-549 human lung cancer and murine P388 lymphocytic leukemia cell lines by SRB and MTT assays, respectively. The results are summarized in Table 2 and show several compounds to be endowed with cytotoxicity in the low micromolar range. And there are two compounds of **1h** and **2e**, which are highly effective against A-549 cell and IC_{50} values are 0.575 and 2.08 μM, respectively.

In addition, we combined the inhibition data of compounds **1** (Table 3) to those of our previously reported 1,4-dihydro-1,2,4,5-tetrazine derivatives (**6**–**37**, Table 3),[12,16–20] and developed CoMFA and CoMSIA 3D-QSAR models.[24,25] Compounds **2** are the 1,2-dihydro structure, so they were not used in 3D-QSAR models. A total of 37 1,4-dihydro-1,2,4,5-tetrazine derivatives, divided into training and test sets, were used for model building and validation, respectively.[26–31] The statistical parameters for CoMFA and CoMSIA models were given in Table 4. The CoMFA model (q^2 = 0.744,

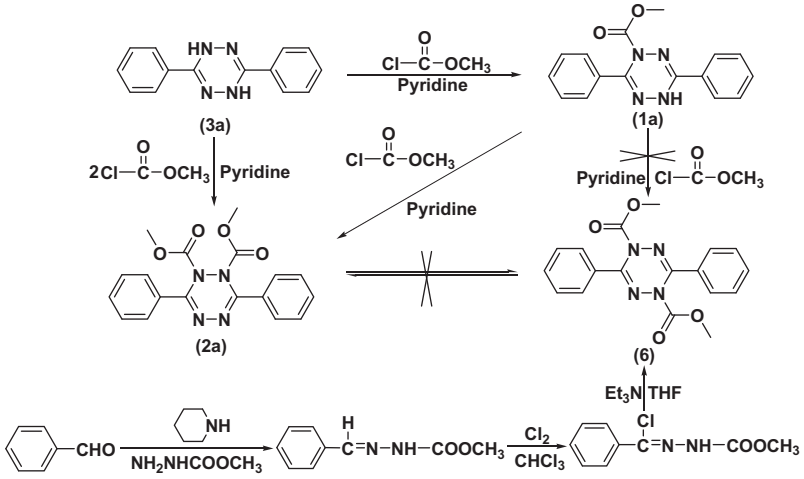

Scheme 2. Synthetic routes of **1a** and **2a**.

Table 3
Chemical structures of 1,2,4,5-tetrazine derivatives used in this study

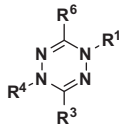

Compd	$R^3 = R^6$	R^1	R^4
1a	Ph	$COOCH_3$	H
1d[a]	Ph	$COO(CH_2)_4CH_3$	H
1e	Ph	$COO(CH_2)_2CH(CH_3)_2$	H
1h[a]	4-$CF_3C_6H_4$	$COOCH_2CH_3$	H
1j	4-ClC_6H_4	$COOCH_3$	H
6[a]	Ph	H	H
7	4-$CF_3C_6H_4$	H	H
8	4-$ClC_6H_4CH_2$	H	H
9	4-ClC_6H_4	H	H
10	2-OH-5-ClC_6H_3	H	H
11	Ph	$COCH_3$	H
12	Ph	$COCH_2CH_3$	H
13[a]	Ph	$COCH(CH_3)_2$	H
14	4-$CF_3C_6H_4$	$COCH_3$	H
15	4-$CF_3C_6H_4$	$COCH_2CH_3$	H
16	4-$CF_3C_6H_4$	$COCH(CH_3)_2$	H
17[a]	Ph	$COCH_2Cl$	H
18	4-$CF_3C_6H_4$	$COCH_2Cl$	H
19	*n*-Pr	CONHPh	CONHPh
20	*n*-Pr	CONH-(3-methylphenyl)	CONH-(3-methylphenyl)
21	*n*-Pr	CONH-(3-chlorophenyl)	CONH-(3-chlorophenyl)
22	Et	CONH-(3-methylphenyl)	CONH-(3-methylphenyl)
23	Me	CONH-(3-methylphenyl)	CONH-(3-methylphenyl)
24	Me	CONH-(3,5-dimethylphenyl)	CONH-(3,5-dimethylphenyl)
25	Me	CONH-(3,5-dimethoxyphenyl)	CONH-(3,5-dimethoxyphenyl)
26[a]	Me	*n*-Bu	*n*-Bu
27	Me	CONH-(3-hydroxyphenyl)	CONH-(3-hydroxyphenyl)
28	Me	CONH-(2-hydroxyphenyl)	CONH-(2-hydroxyphenyl)
29	Ph	CONH-(2-methoxyphenyl)	H
30[a]	3-ClC_6H_4	$COOCH_3$	$COOCH_3$
31	3-$NO_2C_6H_4$	$COOCH_3$	$COOCH_3$
32	4-ClC_6H_4	$COOCH_3$	$COOCH_3$
33	2,4-Dichlorophenyl	$COOCH_3$	$COOCH_3$
34	Ph	Phenylsulfonyl	Phenylsulfonyl
35[a]	4-ClC_6H_4	Phenylsulfonyl	Phenylsulfonyl
36	4-$CH_3OC_6H_4$	Phenylsulfonyl	Phenylsulfonyl
37	Ph	Tosyl	Tosyl

Table 4
Summary of statistical data and validation for CoMFA and CoMSIA models

PLS statistics	CoMFA	CoMSIA
q^2[a]	0.744	0.757
r^2[b]	0.978	0.988
s[c]	0.137	0.101
F[d]	261.501	384.713
ONC[e]	4	5
Steric[f]	0.565	0.102
Electrostatic[g]	0.435	0.298
Donor[h]		0.090
Acceptor[h]		0.336
Hydrophobic[i]		0.174
R^2[j]	0.916	0.898
R_0^2[k]	0.881	0.852
R_0^2[k]	0.909	0.891
$(R^2 - R_0^2)/R^2$	0.038	0.051
$(R^2 - R_0'^2)/R^2$	0.008	0.008
k[l]	0.922	0.922
k'[l]	1.084	1.085

[a] Cross-validated correlation coefficient from LOO.
[b] Noncross-validated r^2.
[c] Standard error of estimate.
[d] *F*-Test value.
[e] Optimum number of principal components.
[f] Steric field contribution.
[g] Electrostatic field contribution.
[h] Donor and acceptor, of hydrogen bond fields, respectively.
[i] Hydrophobic field contribution.
[j] Correlation coefficient is derived from predictions of test set molecules.
[k] Correlation coefficients for regression through the origin for experimental versus predicted and predicted versus experimental activity, respectively.
[l] Slopes for regression through the origin of experimental versus predicted and predicted versus experimental, respectively.

$r^2 = 0.978$) was based on the steric and electrostatic fields, and the CoMSIA model ($q^2 = 0.757$, $r^2 = 0.988$) was based on the steric, electrostatic, hydrophobic, hydrogen bond donor and hydrogen bond acceptor fields. These models revealed a beneficial response to test set validation.[32] Partial least-squares (PLS) analysis was performed to establish a linear relationship between the molecular fields and the activity of molecules.[33–35] The predicted R^2 values of CoMFA and CoMSIA models were found to be 0.916 and 0.898, respectively. Experimental and predicted pIC_{50} values for the training set and test set are reported in Table 5. Figure 3 shows the alignment of all compounds used in the training set. Contour maps for the CoMFA and CoMSIA models are displayed in Figure 4. The relationship between actual and predicted pIC_{50} of the training set and test set compounds of CoMFA and CoMSIA models are illustrated in Figures 5 and 6.

Steric CoMFA contour maps (Fig. 4a) show yellow contours around 3- and 6-positions on tetrazine nucleus indicating that bulky groups are disfavored at these positions. It is confirmed that compounds (**20**, **22**, **23**) substituents in 3- and 6-positions are successively enlarged, in order of decreasing activity. Green contours are close to 1- and 4-positions in the tetrazine nucleus, which suggests that anticancer activity increases with bulky substituents. This explains why compounds (**23**–**25**, **27**, **28**) have better activities than **26**.

Electrostatic CoMFA contour maps (Fig. 4a) are shown in red around 1- and 4-positions on tetrazine nucleus indicating that negative atomic charges might play a favorable role in activity. These compounds (**1h**, **13**–**15**, **17**, **18**, **19**–**25**, **27**) showed higher activity (pIC_{50} >5) owing to the existence of oxygen in the carbonyl group. This trend is different for compounds (**34**–**37**) existence of oxygen in the sulfonyl group, where substituents at 3- and 6-positions play an important role in activity. The blue contour surrounding the substituents at 1- and 4-positions indicates that more positively charged substituents are propitious in these regions. It is confirmed that those compounds (**19**–**25** and **27**) with the amino group in 1- and 4-positions are more potent. And the blue contour around at 3- and 6-positions suggests that positively charged groups are beneficial to increase the activity.

The colors of the steric and electrostatic contour maps in the CoMSIA model (Fig. 4b) have the same meanings as those of the CoMFA model. In agreement with CoMFA, yellow contours and green contours are observed at the same position. Similar to CoMFA, red contours and blue contours are observed at the same position. Unlike CoMFA, the red contour is smaller at the 1- or 4-position, the blue contour is also observed at 3- and 6-positions.

Regions favored by donors and acceptors are shown in cyan and magenta respectively; unfavorable regions are in purple and red, respectively (Fig. 4c). Contours of 1- and 4-positions of the tetrazine nucleus are indicated in cyan, which associated with the amino group of compounds (**19**–**25** and **27**) are more potent. This

Table 5
Experimental and predicted pIC_{50} values of compounds

Compd	Actual IC_{50} (μM)	Actual pIC_{50}[b]	CoMFA		CoMSIA	
			Predicted pIC_{50}[b]	Residual	Predicted pIC_{50}[b]	Residual
1a	39.5	4.403	4.292	0.111	4.284	0.119
1d[a]	40.8	4.389	4.179	0.217	4.265	0.131
1e	44.2	4.355	4.180	0.175	4.312	0.043
1h[a]	0.575	6.240	6.062	0.178	6.109	0.131
1j	49.4	4.306	4.468	−0.156	4.430	−0.118
6[a]	19.9	4.701	4.337	0.364	4.398	0.303
7	40.0	4.398	4.585	−0.187	4.471	−0.073
8	51.8	4.286	4.354	−0.068	4.179	0.107
9	51.8	4.286	4.409	−0.123	4.244	0.042
10	13.2	4.879	4.725	0.154	4.720	0.159
11	44.7	4.350	4.481	−0.131	4.495	−0.145
12	48.3	4.316	4.443	−0.127	4.449	−0.133
13[a]	2.22	5.654	5.529	0.125	5.334	0.320
14	9.76	5.011	4.973	0.038	4.984	0.027
15	9.56	5.020	4.982	0.038	5.008	0.012
16	31.6	4.500	4.367	0.133	4.545	−0.045
17[a]	1.85	5.733	5.505	0.228	5.423	0.310
18	8.53	5.069	4.985	0.084	5.029	0.040
19	5.42	5.266	5.341	−0.075	5.153	0.113
20	1.00	6.000	6.119	−0.119	6.209	−0.209
21	1.10	5.959	5.863	0.096	5.923	0.036
22	0.639	6.194	6.284	−0.090	6.301	−0.107
23	0.574	6.241	6.048	0.193	6.226	0.015
24	3.66	5.437	5.193	0.244	5.354	0.083
25	0.0350	7.456	7.434	0.022	7.371	0.085
26[a]	68.5	4.164	4.515	−0.351	4.518	−0.354
27	5.55	5.256	5.469	−0.213	5.196	0.060
28	57.3	4.242	4.348	−0.106	4.206	0.036
29	44.9	4.348	4.334	0.014	4.282	0.066
30[a]	89.0	4.051	4.342	−0.291	4.415	−0.364
31	83.6	4.078	4.026	0.052	4.205	−0.127
32	76.7	4.115	4.052	0.063	4.118	−0.003
33	79.3	4.101	4.118	−0.017	4.179	−0.078
34	74.1	4.130	4.282	−0.152	4.120	0.010
35[a]	51.9	4.285	4.330	−0.045	4.094	0.191
36	58.8	4.231	4.213	0.018	4.264	−0.033
37	85.8	4.067	3.935	0.132	4.043	0.024

[a] Compounds in the test set.
[b] $pIC_{50} = -\log(IC_{50})$.

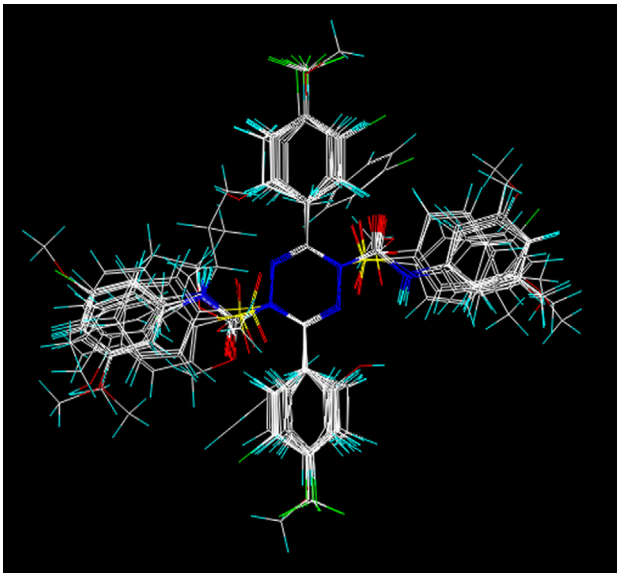

Figure 3. Alignment of all compounds in the training set.

observation is in agreement with blue CoMFA electrostatic contours in the same area (Fig. 4a). The magenta favorable hydrogen bond acceptor contour is shown at 1- and 4-positions and is associated with the carbonyl group of compounds (**1h**, **13**–**15**, **17**, **18**, **19**–**25**, **27**) which showed higher activity (pIC_{50} >5). This contour is in agreement with the CoMFA and CoMSIA red electrostatic contour in the same region (Fig. 4a and b).

Hydrophobic contour maps (Fig. 4d) show gray around 3- and 6-positions on tetrazine nucleus indicating that hydrophobic groups are disfavored at these positions. The contour can be explained by the presence of the substituted phenyl, which in most cases produces less active compounds. This contour is in agreement with the yellow contour at the same position in CoMFA and CoMSIA steric contour maps (Fig. 4a and b). Two favorable yellow regions are observed at 1- and 4-positions, similar to the green contour at the same position in CoMFA and CoMSIA steric contour maps (Fig. 4a and b).

The analysis of contour maps for CoMFA and CoMSIA models indicates that larger groups at 3- and 6-positions with hydrophobic segments generate less active compounds. Substitutions at 3- and 6-positions with methyl are favored over other substitutions in the current data set. Also, carbonyl group at 1- and 4-positions can generate regions with negative charges that could act as hydrogen bond acceptors and the amino group of 1- and 4-positions can generate areas with positive charges that could act as hydrogen bond donors involving the binding site. In general, bulky groups at 1- and 4-positions play favorable roles in activity.

In conclusion, 3,6-diaryl-dihydro-1,2,4,5-tetrazine derivatives were synthesized. They were confirmed by single-crystal X-ray diffraction and evaluated against A-549 and P388 cells in vitro.

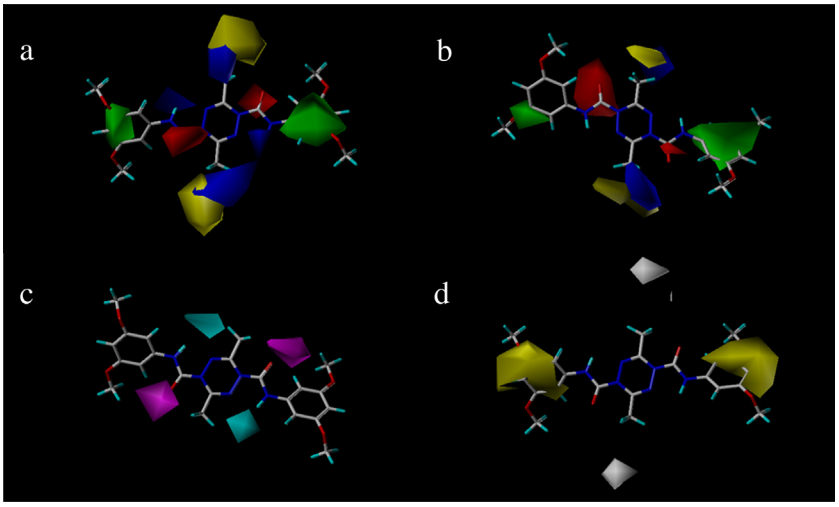

Figure 4. CoMFA and CoMSIA STDEV*COEFF contour maps. CoMFA model: (a) sterically favored areas are in green, and sterically disfavored areas are in yellow; negative charge favored areas are in red and disfavored areas are in blue. CoMSIA model: The colors in (b) have the same meanings as do CoMFA contour maps. (c) donor and acceptor favored areas are in cyan and magenta, respectively, and donor and acceptor disfavored areas are in purple and red, respectively. (d) hydrophobic favored areas are in yellow and disfavored areas in gray.

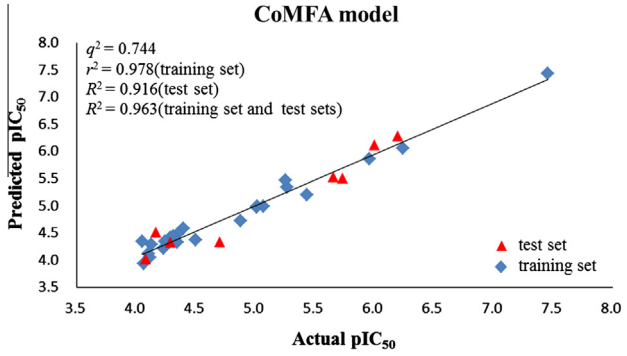

Figure 5. Plot of observed versus predicted activities for the training and test set compounds based on the CoMFA model.

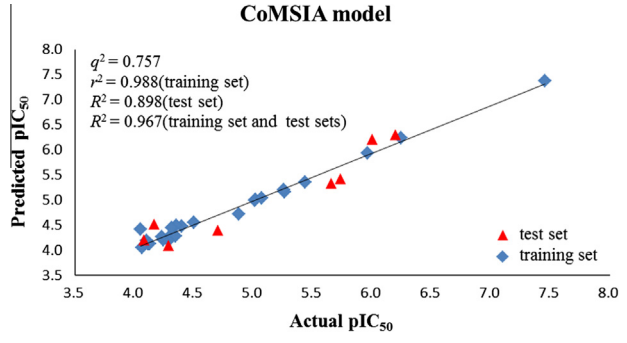

Figure 6. Plot of observed versus predicted activities for the training and test set compounds based on the CoMSIA model.

Monosubstituted dihydrotetrazines are the 1,4-dihydro structure, but disubstituted dihydrotetrazines are the 1,2-dihydro structure. There may be a rearrangement during the synthesis process of disubstituted dihydrotetrazines. The results of their antitumor activities show several compounds to be endowed with cytotoxicity in the low micromolar range and there are two compounds of **1h** and **2e**, which are highly effective against A-549 cell and IC_{50} values are 0.575 and 2.075 μM, respectively. CoMFA and CoMSIA 3D-QSAR models were generated, showed good q^2 and r^2 values and revealed a beneficial response to test set validation. These models provide the tool for guiding the design and synthesis of novel and more potent tetrazine derivatives.

Acknowledgments

The authors are very grateful to the National Natural Science Foundation of China (No. 20802069) and the Natural Science Foundation of Zhejiang Province (No. Y2090985) for financial support and the National Center for Drug Screening of China for evaluation of antitumor activities.

Supplementary data

Supplementary data associated with this article can be found, in the online version, at http://dx.doi.org/10.1016/j.bmcl.2013.09.036.

References and notes

1. Falfushynska, H. I.; Gnatyshyna, L. L.; Stoliar, O. B. *Comp. Biochem. Physiol., Part C: Toxicol. Pharmacol.* **2012**, *155*, 396.
2. Zhu, Y.-Q.; Cheng, J.; Zou, X.-M.; Hu, F.-Z.; Xiao, Y.-H.; Yang, H.-Z. *Chin. J. Org. Chem.* **2008**, *28*, 1044.
3. Nhu, D.; Duffy, S.; Avery, V. M.; Hughes, A.; Baell, J. B. *Bioorg. Med. Chem. Lett.* **2010**, *20*, 4496.
4. Pandey, V. K. *Indian Drugs* **1986**, *23*, 500.
5. Sharma, P.; Kumar, A.; Sahu, V.; Singh, J. *Arkivoc (Gainesville, FL, US)* **2008**, 218.
6. Tabassum, S.; Parveen, M.; Ali, A.; Alam, M.; Ahmad, A.; Khan, A. U.; Khan, R. A. *J. Mol. Struct.* **2012**, *1020*, 33.
7. Sauer, J. In *Comprehensive Heterocyclic Chemistry II*; Katritzky, A. R., Rees, C. W., Scriven, E. F. V., Eds.; Pergamon: Oxford, 1996; Vol. 6, p 901.
8. Stanovnik, B.; Grošelj, U.; Svete, J. In *Comprehensive Heterocyclic Chemistry III*; Katritzky, A. R., Ramsden, C. A., Scriven, E. F. V., Taylor, R. J. K., Eds.; Elsevier, 2008; Vol. 9, p 641.
9. Neunhoeffer, H. In *Comprehensive Heterocyclic Chemistry*; Katritzky, A. R., Rees, C. W., Eds.; Pergamon: Frankfurt, 1984; Vol. 3, p 531.
10. Eremeev, A. V.; Tikhomirov, D. A.; Tyusheva, V. A.; Liepins, E. *Khim. Geterotsikl* **1978**, 753.
11. Calahorro, A. J.; Penas-Sanjuan, A.; Melguizo, M.; Fairen-Jimenez, D.; Zaragoza, G.; Fernandez, B.; Salinas-Castillo, A.; Rodriguez-Dieguez, A. *Inorg. Chem.* **2013**, *52*, 546.
12. Rao, G. W.; Guo, Y. M.; Hu, W. X. *ChemMedChem* **2012**, *7*, 973.
13. Qiu, L. N.; Zhou, Y. L.; Wang, Z. N.; Huang, Q.; Hu, W. X. *Int. J. Oncol.* **2012**, *41*, 533.
14. Sharma, H.; Cheng, X.; Buolamwini, J. K. *J. Chem. Inf. Model.* **2012**, *52*, 515.
15. Sivan, S. K.; Manga, V. *J. Mol. Model.* **2012**, *18*, 569.
16. Rao, G. W.; Hu, W. X. *Bioorg. Med. Chem. Lett.* **2006**, *16*, 3702.

17. Lv, L. P. Zhejiang University of Technology, 2006.
18. Hu, W. X.; Lv, L. P.; Xu, F.; Shi, H. B. *J. Chem. Res-S* **2006**, *30*, 324.
19. Rao, G. W.; Hu, W. X. *Bioorg. Med. Chem. Lett.* **2005**, *15*, 3174.
20. Hu, W. X.; Rao, G. W.; Sun, Y. Q. *Bioorg. Med. Chem. Lett.* **2004**, *14*, 1177.

21. *Synthesis of compound* ***1g***: 3,6-Bis(4-trifluoromethylphenyl)-1,4-dihydro-1,2,4,5-tetrazine (**3b**, 5 mmol), prepared according to the procedure of Rao and Hu[16] from 4-(trifluoromethyl)benzonitrile and hydrazine hydrate, was dissolved in dichloromethane (20 mL) with stirring under nitrogen protection in an ice bath. Pyridine (0.5 mL) was added to the mixture. Methyl chloroformate (5 mmol) and dichloromethane (20 mL) were added dropwise into the mixture under 0–5 °C. The mixture was stirred at room temperature for 24 h, then washed in water and dried with anhydrous $MgSO_4$. The solvent was removed in vacuo and the residue was recrystallized from 95% ethanol to give the product (**1g**) as a yellow solid (yield 53.7%). A solution of the compound in ethanol was concentrated gradually at room temperature to afford yellow prisms which are suitable for X-ray diffraction, mp: 198–199 °C; ^{1}H NMR (400 MHz, $CDCl_3$): δ 3.83 (s, 3H), 7.67–7.73 (m, 6H), 7.89–7.91 (m, 2H), 8.07 (s, 1H); IR ν_{max} (KBr)/cm^{-1}: 3312, 3085, 2972, 1689, 1618, 1573, 1522, 1475, 1448, 1378, 1327, 851; MS (EI, 70 eV): *m*/*z* (%): 430 (22) [M]$^+$, 386 (12), 186 (14), 172 (100), 145 (44), 95 (13), 75 (12), 59(34); Anal. Calcd (%) for $C_{18}H_{12}N_4O_2F_6$: C, 50.24; H, 2.81; N, 13.02. Found: C, 50.28; H, 2.66; N, 13.16. Compounds of **1a–j** were synthesized in the same manner. Synthesis of compound **2g**: 3,6-Bis(4-trifluoromethylphenyl)-1,4-dihydro-1,2,4,5-tetrazine (**3b**, 5 mmol), prepared according to the procedure of Rao and Hu[16] from 4-(trifluoromethyl) benzonitrile and hydrazine hydrate, was dissolved in dichloromethane (20 mL) with stirring under nitrogen protection in an ice bath. Pyridine (1 mL) was added to the mixture. Propyl chloroformate (10 mmol) and dichloromethane (20 mL) were added dropwise into the mixture under 0–5 °C. The mixture was stirred at room temperature for 16 h, then washed in water and dried with anhydrous $MgSO_4$. The solvent was removed in vacuo and the residue was recrystallized from ethanol/dichloromethane (1:1) to give the product (**2g**) as a colourless solid (yield 52.7%). A solution of the compound in ethanol was concentrated gradually at room temperature to afford colourless prisms which are suitable for X-ray diffraction, mp: 147–149 °C; ^{1}H NMR (400 MHz, $CDCl_3$): δ 0.64 (t, 6H), 1.46–1.48 (m, 4H), 4.04–4.19 (m, 4H), 7.77 (d, *J* = 8.2 Hz, 4H), 8.18 (d, *J* = 8.1 Hz, 4H); IR ν_{max} (KBr)/cm^{-1}: 2975, 2886, 1759, 1618, 1545, 1501, 1467, 1321, 1263, 1215, 854; MS (EI, 70 eV): *m*/*z* (%): 545 (13) [M+H]$^+$, 546 (3), 459 (4), 414 (2), 172 (3), 44 (4), 76 (18), 43 (100), 41 (51); Anal. Calcd (%) for $C_{24}H_{22}N_4O_4F_6$: C, 52.95; H, 4.07; N, 10.29. Found: C, 53.02; H, 3.99; N, 10.31. Compounds of **2a–i** were synthesized in the same manner. Data for other compounds are provided in the Supplementary data.
22. *Crystal data of compound* ***1g***: A yellow prism of dimensions 0.35 × 0.25 × 0.25 mm^3 was used for data collection with an Enraf-Nonius CAD-4 diffractometer with graphite monochromated MoKα radiation (λ = 0.71073 Å). The structure was solved by direct method procedures as implemented in the SHELXS97[23] program. The positions of all the non-hydrogen atoms were included in the full-matrix least-squares refinement using the SHELXS97[23] program. Hydrogen atoms were added at calculated positions and refined using a riding model; they were given isotropic displacement parameters equal to 1.2 (or 1.5 for methyl H atoms) times the equivalent isotropic displacement parameters of their parent atoms, and C–H distances were restrained to 0.96 Å for methyl H atoms and 0.93 Å for phenyl H atoms, while N–H distances were set to 0.86 Å. $C_{18}H_{12}F_6N_4O_2$, M_r = 430.32, monoclinic, *a* = 9.177(3), *b* = 12.159(2), *c* = 16.896(2) Å, β = 104.540(16)°, *U* = 1824.9(6) Å^3, *T* = 298(2) K, space group: $P2_1/c$, *Z* = 4, ρ_{calcd} = 1.566 g cm^{-3}, μ(MoKα) = 0.146 mm^{-1}, 3839 reflections measured, 3269 unique (R_{int} = 0.0194) which were used in all calculations. Fine R_1 = 0.0307, *wR* (F^2) = 0.0939 (all data). All crystallographic details for compound **1g** have been deposited with the Cambridge Crystallographic Data Centre: CCDC-255697 contains the supplementary crystallographic data for this Letter.
Crystal data of compound ***2g***: A colorless prism of dimensions 0.35 × 0.25 × 0.25 mm^3 was used for data collection with an Enraf-Nonius CAD-4 diffractometer with graphite monochromated MoKα radiation (λ = 0.71073 Å). The structure was solved by direct method procedures as implemented in the SHELXS97[23] program. The positions of all the non-hydrogen atoms were included in the full-matrix least-squares refinement using the SHELXS97[23] program. Hydrogen atoms were added at calculated positions and refined using a riding model; they were given isotropic displacement parameters equal to 1.2 (or 1.5 for methyl H atoms) times the equivalent isotropic displacement parameters of their parent atoms, and C–H distances were restrained to 0.96 Å for methyl H atoms, 0.97 Å for methylene H atoms, and 0.93 Å for phenyl H atoms. $C_{24}H_{22}F_6N_4O_4$, M_r = 544.46, triclinic, *a* = 8.210(2), *b* = 12.151(2), *c* = 14.469(3) Å, α = 107.860(14)°, β = 100.640(19)°, γ = 99.570(19)°, *U* = 1311.4(5) Å^3, *T* = 298(2) K, space group: $P\bar{1}$, *Z* = 2, ρ_{calcd} = 1.379 g cm^{-3}, μ(MoKα) = 0.123 mm^{-1}, 5777 reflections measured, 4707 unique (R_{int} = 0.0140) which were used in all calculations. Fine R_1 = 0.0530, *wR* (F^2) = 0.2036 (all data). All crystallographic details for compound **2g** have been deposited with the Cambridge Crystallographic Data Centre: CCDC-255700 contains the supplementary crystallographic data for this Letter.

23. Sheldrick, G. M. *Acta Crystallogr., Sect. A* **2008**, *64*, 112.

24. CoMFA studies were performed with SYBYL 6.9.1 molecular modeling software.[25] Steric and electrostatic interactions were calculated using a sp^3 carbon probe atom with a charge of +1 with a distance-dependent dielectric at each lattice point, and energy cut-off of 30 kcal mol^{-1}. Each molecule was calculated on a 3D cubic lattice with grid spacing of 2 Å in *x*, *y*, and *z* directions. The CoMFA-STD method in SYBYL was used to scale CoMFA fields. Similarity indices were derived from the same lattice box, which were utilized in CoMFA calculations. Steric, electrostatic, hydrophobic, hydrogen bond donor and hydrogen bond acceptor descriptors were evaluated using the probe atom. GAUSSIAN-type distance dependence was used to measure the relative attenuation of the field position of each atom in the lattice and a default value of 0.3 was used as the attenuation factor.

25. SYBYL 6.9.1, Tripos Inc.: St. Louis, MO, 2003.

26. The IC_{50} (concentration causing 50% inhibitory effect on the A549 proliferation) values were converted to pIC_{50} ($-\log IC_{50}$) values and used as dependent variables in the CoMFA and CoMSIA QSAR analysis. For 3D-QSAR analyses, 29 compounds (78.4%) were selected as the training set for model construction, and the remaining 8 compounds (21.6%) as the test set for model validation. The activities of the training set range from 0.035 μM (pIC_{50} = 7.456) to 85.806 μM (pIC_{50} = 4.066). The activities of the test set range from 0.575 μM (pIC_{50} = 6.240) to 88.988 μM (pIC_{50} = 4.051). The fact worth mentioning is that the structural diversity and activity range of the test set are comparable with the training set.[27–29] In the development of 3D-QSAR models, the molecular alignment and conformation selection are the most essential steps. Conformations of each compound were generated using Confort™ conformation analysis. Energy minimizations were performed using Tripos force field[30] with a distance-dependent dielectric and Powell conjugate gradient algorithm with a convergence criterion of 0.005 kcal/(mol Å). Gasteiger–Hückel[31] charges were assigned to all molecules. Since specific molecular target is unknown to these compounds, the most active compound **25** was used as a template for superimposition, assuming that its conformation represents the most bioactive conformation of the tetrazine derivatives. All compounds were aligned using a tetrazine nucleus as common substructure in all molecules and minimum scaffold required for active molecules. Figure 3 shows the alignment of all compounds in the training set.

27. Golbraikh, A.; Shen, M.; Xiao, Z. Y.; Xiao, Y. D.; Lee, K. H.; Tropsha, A. *J. Comput. Aided Mol. Des.* **2003**, *17*, 241.
28. Golbraikh, A.; Tropsha, A. *J. Mol. Graph. Model.* **2002**, *20*, 269.
29. Golbraikh, A.; Tropsha, A. *J. Comput. Aided Mol. Des.* **2002**, *16*, 357.
30. Clark, M.; Cramer, R. D., III; Van, O. N. *J. Comput. Chem.* **1989**, *10*, 982.
31. Gasteiger, J.; Marsili, M. *Tetrahedron* **1980**, *36*, 3219.

32. Validation was carried out considering the q^2 coefficient and predicting the activity of an external test set with 8 compounds. According to Golbraikh and Tropsha,[28,29] models are considered highly predictive if they satisfy all of the following conditions (I–IV):
I. $q^2 > 0.5$
II. $R^2 > 0.6$
III. $[(R^2 - R_0^2)/R^2)] < 0.1$ or $[((R^2 - R_0'^2)/R^2)] < 0.1$
IV. $0.85 \leqslant k \leqslant 1.15$ or $0.85 \leqslant k' \leqslant 1.15$
where, q^2 is the cross-validated correlation coefficient from LOO; R^2 is the correlation coefficient for experimental (y) versus predicted ($\tilde{y}$) activities for test set molecules; R_0^2 and $R_0'^2$ are the correlation coefficients of the regression through the origin for y versus ($\tilde{y}$) and ($\tilde{y}$) versus y, respectively; k and k' are the slopes for regression through origin $y^{r0} = k\tilde{y}$ and $\tilde{y}^{r0} = k'y$ and were calculated as follows:

$$k = \frac{\sum y_i \tilde{y}_i}{\sum \tilde{y}_i^2}$$

$$k' = \frac{\sum y_i \tilde{y}_i}{\sum y_i^2}$$

33. PLS,[34,35] the statistical method used in deriving the 3D-QSAR models, implemented in SYBYL 6.9.1 was used to generate a linear regression that correlates descriptors with biological activities in pIC_{50}, cross validation being used to obtain the optimum number of the principal components. The cross-validation analysis was performed utilizing the leave-one-out (LOO) method in which one compound was removed from the data set and its activity was predicted using the model built from the rest of the data set. The cross-validated coefficient q^2 was evaluated as:

$$q^2 = 1 - \frac{\sum (Y_{pred} - Y_{exp})^2}{\sum (Y_{exp} - Y_{mean})}$$

where Y_{pred}, Y_{exp} and Y_{mean} are the predicted, experimental and mean values of the pIC_{50}, respectively.

34. Bush, B. L.; Nachbar, R. B., Jr. *J. Comput. Aided Mol. Des.* **1993**, *7*, 587.
35. Clark, M.; Cramer, R. D. *Quant. Struct. Act. Relat.* **1993**, *12*, 137.